

Mapping Thunder Sources by Inverting Acoustic and Electromagnetic Observations

by

Jacob Anderson

Submitted in Partial Fulfillment
of the Requirements for the Degree of
Master of Science in Geophysics (Solid Earth)

New Mexico Institute of Mining and Technology
Socorro, New Mexico

February, 2013

ABSTRACT

I present a new method of precisely locating current flow in lightning strikes by joint inversion of electromagnetic data from a Lightning Mapping Array and recorded thunder signals. First, radio frequency (RF) pulses are connected to reconstruct conductive channels created by leaders. Then, acoustic signals that would be produced by current flow through each channel are forward-modeled. The recorded thunder is considered to consist of a weighted superposition of these acoustic channels. I calculate the posterior distribution of acoustic source energy for each channel with a Markov Chain Monte Carlo inversion that fits power envelopes of modeled and recorded thunder. Quality of results is affected by factors like atmospheric turbulence, topographic reflections, uncertainty in RF pulse locations provided by the LMA, and atmospheric winds; I examine the latter two in detail. I apply this method to several lightning flashes over the Magdalena Mountains, New Mexico. This method will enable more detailed study of lightning phenomena by allowing researchers to map current flow in addition to leader propagation.

ACKNOWLEDGMENTS

I first acknowledge the advice and guidance provided by my advisor, Jeff Johnson, and my committee. Their suggestions led to many breakthroughs and improved the paper. I thank R. Arechiga and R. Johnson for many enlightening discussions. J. Chaput was an essential mentor throughout this project, for whose frequent, helpful, and patient advice I am grateful. R. Arechiga, E. Badillo, J. Johnson, R. Johnson, J. Michnovicz, and M. Murray participated in fieldwork, and H. Edens provided RF pulse locations from the LMA. This work was funded by NSF grant AGS-0934472.

This thesis was typeset with \LaTeX^1 by the author.

¹The \LaTeX document preparation system was developed by Leslie Lamport as a special version of Donald Knuth's \TeX program for computer typesetting. \TeX is a trademark of the American Mathematical Society. The \LaTeX macro package for the New Mexico Institute of Mining and Technology thesis format was written for the Tech Computer Center by John W. Shipman.

CONTENTS

LIST OF FIGURES	v
1. INTRODUCTION	1
2. DESCRIPTION OF METHOD	6
2.1 Conductive Channel Identification	6
2.2 Acoustic Forward Modeling	8
2.3 Inversion for Channel Source Amplitudes	9
3. EXPERIMENT	13
3.1 Deployment and Data	13
3.2 Results	16
3.2.1 19:42:13 Flash	16
3.2.2 19:06:36 Flash	19
3.2.3 19:14:41 Flash	19
3.2.4 19:32:51 Flash	19
3.2.5 19:50:08 Flash	22
3.2.6 19:54:19 Flash	22

4. SENSITIVITY OF METHOD TO SOURCES OF ERROR	26
4.1 Sensitivity to RF pulse location noise	26
4.2 Sensitivity to atmospheric simplification	27
5. DISCUSSION	31
6. CONCLUSION	34
REFERENCES	36

LIST OF FIGURES

2.1	Schematic outline of the inversion method, using synthetic data. A: each RF pulse is connected to its nearest neighbor that occurs earlier in time. These connections can be traced backwards to reconstruct conductive channels. B: each channel (here, channel 3) is discretized as a set of finely spaced interpolated acoustic sources. Travel times and amplitudes are calculated for waves propagating from each source to the receiver. These arrivals are represented as time-shifted, amplitude-scaled delta functions, and are superposed to form an arrival function. C: arrival functions are filtered, and the power envelope is calculated for the filtered recorded data. D: a nonlinear inversion is performed to match the power envelope of a weighted superposition of filtered arrival functions to the power envelope of the recorded data.	11
2.2	The number of channels in a flash can be reduced by discarding those with short independent length. This reduces the computational expense of forward-modeling thunder signals, as well as reducing the number of free parameters in the inverse problem. In this flash, the number of channels to consider was reduced from 431 to 7.	12

3.1	Map of sensor deployment used in this experiment in central New Mexico, USA. The LMA (A) consisted of a “regional” component consisting of six antennas spaced around the Magdalena Mountains at distances of more than 10 km and a “local” component including three antennas deployed close together high in the mountains. The acoustic network (B) included three broadband microphones deployed in the same area as the local part of the LMA (within the blue square). The MGTM station is used as the origin of the map.	14
3.2	A: Overlay of modeled and recorded thunder power envelopes for the CG flash at 19:42:13. B: Map of inverted channel energy densities. C: Posterior distributions of channel energy densities of thunder-producing channels. Channel 4, which is the direct channel to ground, produces the most thunder. Channels 2 and 5, which connect channel 4 to higher parts of the strike, produce little thunder.	17
3.3	The evolution of the CG flash at 19:42:13 with time. Color of plotted points corresponds to VHF pulse times. Black vertical lines indicate times of major low-frequency radio pulses from return strokes; gray lines indicate smaller radio pulses. Most of the upper channels formed after the return strokes, making them unlikely to produce significant thunder.	18

3.4	A: Overlay of modeled and recorded thunder power envelopes for the IC flash at 19:06:36. B: Map of inverted channel energy densities for the flash. C: Posterior distributions of channel energy densities of thunder-producing channels. Channels 1 and 2 are somewhat correlated; this is a potential source of ambiguity in the results.	20
3.5	A: Overlay of modeled and recorded thunder power envelopes for the 19:14:41 CG flash. B: Map of inverted channel energy densities. The ground strike has the highest energy density; however, thunder is also detected from two upper channels. C: Posterior distributions of energy densities of thunder-producing channels. Energy densities of two upper channels are correlated, making distinguishing thunder from those channels difficult.	21
3.6	A: Overlay of modeled and recorded thunder power envelopes for the 19:32:51 IC flash. B: Map of inverted channel energy densities. Most energy is released by a high-elevation channel, but small amounts are also produced by other channels. C: Posterior distributions of channel energy densities of thunder-producing channels.	23
3.7	A: Overlay of modeled and recorded thunder power envelopes for the 19:50:08 IC flash. B: Map of inverted channel energy densities. C: Posterior distributions of channel energy densities of thunder-producing channels. Only one channel is found to produce any thunder.	24

3.8	A: Overlay of modeled and recorded thunder power envelopes for the 19:54:19 IC flash. B: Map of inverted channel energy densities. C: Posterior distributions of channel energy densities of thunder-producing channels. An upper channel (3) produces most thunder; contributions from the lower channel (2) are smaller and poorly resolved.	25
4.1	Contours showing the effect of LMA RF pulse location noise on inversions of synthetic data. Monte Carlo simulations revealed effects on (A) fractional misfit between pre-noise and post-noise synthetic thunder and (B) errors between true and inverted amplitude (expressed as root-mean-square residual between true and inverted amplitudes). Fractional thunder misfits increase with both the RMS location error and the corner frequency. However, errors in inverted channel amplitudes depend more strongly on RMS location error than on corner frequency.	28
4.2	Effect of atmospheric wind intensity on (A) fractional misfit between true synthetic and inverted synthetic thunder and (B) accuracy of inverted channel amplitudes. Thunder misfit increases with corner frequency and maximum surface wind. However, true channel amplitudes can still be recovered reasonably accurately for low frequency bands.	30

This thesis is accepted on behalf of the faculty of the Institute by the following committee:

Jeff Johnson, Advisor

I release this document to the New Mexico Institute of Mining and Technology.

Jacob Anderson

Date

CHAPTER 1

INTRODUCTION

Thunderstorms are powerful phenomena with far-reaching effects of interest both practical (such as hazards to life and property) and scientific (like powering the global electric circuit) (*Rakov and Uman, 2003*). They form from the rapid upward advection of moist air to high, cold elevations, where water vapor condenses and precipitates. They undergo three basic stages in their development: a growth stage dominated by an updraft that carries moist air upward to form a cumulus cloud; a mature stage in which falling precipitation entrains unstable cold air to form a strong local downdraft; and a dissipation stage dominated by widespread downdrafts that deplete the cloud (*Byers and Braham, 1948*).

Unstable air is required to form the updrafts that fuel a thunderstorm. Air is considered unstable when a parcel displaced upward continues to rise indefinitely because the rate at which it cools by decompression (the adiabatic lapse rate) is less than the vertical gradient in air temperature (the environmental lapse rate), ensuring that it remains warmer and less dense than its surroundings as it ascends. Therefore, a strong vertical temperature gradient is a prerequisite for thunderstorm formation (*Byers and Braham, 1948*). Wind shear also plays an important role by spatially separating the precipitation and downdraft from the pre-existing updraft. When the wind shear is weak, precipitation falls through the updraft, weakening it and causing the storm to dissipate quickly. A stronger

wind shear prevents this and results in a more long-lived and powerful storm. However, excessive wind shear can tear apart the updraft, preventing the storm from forming in the first place (*Weisman and Klemp, 1982*).

Two types of solid precipitation—ice crystals and graupel—are present in thunderstorm clouds. Collisions between these particles deposit negative charge on graupel and positive charge on ice. Graupel particles are much larger and heavier than ice crystals, and therefore fall faster; the differential motion of these two types of precipitation results in positive ice crystals creating a net positive charge at high elevations in the cloud, and negative graupel creating a net negative charge lower in the cloud (*Reynolds et al., 1957; Berdeklis and List, 2001*). Lightning discharges can then occur between the two charge layers in the cloud, or between one of them and the ground (*Rakov and Uman, 2003*).

Lightning strikes begin with the propagation of ionized channels called stepped leaders in areas with strong electric fields. These leaders grow through series of ionization events (called steps) which lengthen the ionized channel in random directions beyond the original extent. These steps are separated by several microseconds in time and tens of meters in space. In this manner, leaders form tortuous, dendritic structures that are electrically conductive (*Uman, 1987*). Any of these conductive channels may carry current, but few typically do; only 35% of one study's cloud-ground flashes were observed to contain more than a single current-carrying channel (*Valine and Krider, 2002*).

Audible and near-infrasonic thunder is produced mainly by rapid heating of conductive lightning channels in response to current flow (*Few, 1969*). During a typical lightning strike, a current pulse on the order of 3×10^4 A travels along conductive channels. This current rapidly heats the surrounding air (3×10^4

K in 5×10^{-6} s) and raises the surrounding pressure to around 10^6 Pa. Such an intense overpressure forms a shock wave that propagates supersonically (up to 3300 ms^{-1}) (Rakov and Uman, 2003). While additional shock waves may be generated by subsequent strokes, the time separating these strokes (on the order of 4×10^{-2} s) is enough so shock waves from different strokes are sufficiently far apart as to not interact with each other (Few, 1974). These shock waves quickly decay to acoustic waves. As a result, each stroke radiates acoustic waves along the length of the current-carrying channel. Recordings of these acoustic waves show that intracloud strikes tend to produce thunder with lower amplitudes and peak frequencies than cloud-ground strikes (Holmes et al., 1971; Johnson, 2012).

For frequencies below about 2.5 Hz, thunder is dominated by an electrostatic relaxation of the cloud instead of by rapid thermal expansion (Balachandran, 1979). Before a strike can occur, a substantial charge must accumulate in a cloud. Electrostatic forces cause these charged particles to repel each other. When current flow in lightning depletes these charges, the electrostatic repulsion forces decrease, and charged particles are drawn inward. This implosive movement produces a low-frequency planar rarefaction wave that propagates downward from the cloud and is most commonly observed directly below storms (Balachandran, 1979, 1983; Bohannon et al., 1977). This paper will focus on modeling and locating thermal expansion thunder sources instead of this electrostatic relaxation source.

Previous studies have attempted to locate thunder sources by obtaining wavenumber vectors from array recordings, finding lightning strike time from electromagnetic observations, and backpropagating the thunder recordings accordingly (Few, 1970; Few and Teer, 1974; Teer and Few, 1974; MacGorman et al., 1981; Arechiga et al., 2011; Johnson et al., 2011). The general shapes and locations

of thunder sources from the last two studies were confirmed by comparison to maps of RF pulses from leaders. However, the raypaths (and backpropagated source locations) are sensitive to atmospheric temperature and wind structure, which is typically poorly constrained. Consequently, acoustic data alone cannot unambiguously reveal thunder source locations.

The New Mexico Tech Lightning Mapping Array (LMA) has proven a valuable tool for studying lightning over the past decade. The LMA consists of networked antennas that detect and locate RF pulses produced by ionization events in stepped leaders (*Rison et al., 1999*). Accuracy of these pulse locations is around 10 m in the horizontal directions and around 30 m vertically (*Thomas et al., 2004*). These pulses are vertices in the stepped leader structure, and can therefore be used to reconstruct the leaders. Knowledge of the stepped leader structure of the strike is useful in modeling thunder because audible and near-infrasonic thunder comes from current flow along some subset of these channels. Therefore, LMA pulse locations are used to constrain thunder source locations in this method.

Acoustic modeling requires knowledge of the propagation medium's structure. Unfortunately, thunderstorm atmospheric structures can be complicated and difficult to measure. Storms require unstable air to form and persist, so the temperature lapse rate in a thunderstorm must exceed the adiabatic lapse rate ($5 - 10^{\circ}\text{C km}^{-1}$, depending on humidity). Because the intrinsic sound speed of air is proportional to the square root of temperature, sound speed must also decrease with elevation, which causes acoustic waves to be refracted upward. Consequently, thunder is rarely heard more than 25 km from a flash because refraction prevents the thunder from reaching the ground beyond that point (*Fleagle,*

1949). On the other hand, low-level structures below the storm, such as inversions, could amplify thunder generated at low elevations.

Additionally, thunderstorms often include intense and sheared wind. Wind affects the speed at which sound propagates and can have refractive effects of equal importance to those of the temperature lapse rate (*Fleagle, 1949*). Refraction from wind and temperature in these heterogeneous, anisotropic structures affects arrival time and amplitude of acoustic waves. Because thunderstorm temperature and wind information is not commonly only available above the surface, predicting refractive effects on thunder signals is generally not possible.

Other propagation effects further alter thunder signals. Amplitudes of thunder acoustic waves within roughly the first kilometer of propagation are high enough to make the wave behave nonlinearly (*Otterman, 1959*), resulting in lengthening of waves. Turbulence is another common complication of thunderstorm atmospheres, although its consequences to sound wave propagation are difficult to quantify. Multipathing by topographic scattering can further complicate thunder; however, due to the computational expense of calculating reflected ray paths, and the lower amplitudes of scattered waves compared to direct arrivals, it is not considered here. Another factor (mainly affecting high frequencies) is intrinsic attenuation, which dissipates energy in acoustic waves. Attenuation is roughly equal to an elevation-dependent coefficient times frequency squared, and it never exceeds 7.35×10^{-2} dB/km over the low elevations and frequencies studied here (less than 24 Hz, less than 12 km) (*Sutherland and Bass, 2004; de Groot-Hedlin, 2008*). The flashes studied here occur within 12 km of the microphones, so no interesting part of our signals is ever attenuated by more than 2 dB, and the bulk of the signals is attenuated much less than that. Because the effect of attenuation on our signals is weak, it is not considered here.

CHAPTER 2

DESCRIPTION OF METHOD

This inversion method locates and quantifies thunder generation in lightning flashes (Figure 2.1). It requires RF pulse locations (computed by the LMA) and acoustic recordings of thunder. I identify conductive channels by connecting RF pulses (Section 2.1), and, assuming some reasonable atmosphere, forward model the acoustic signal that would be recorded for each conductive channel (Section 2.2). Treating the thunder as a weighted superposition of the channels' acoustic signatures, I then invert to find the acoustic amplitude of each channel that optimizes the fit of modeled thunder power envelopes to recorded thunder power envelopes (Section 2.3). Because the true structure of the atmosphere around the strike is unknown, I repeat this process many times over many reasonable atmospheres until an optimal fit is found.

2.1 Conductive Channel Identification

The LMA provides a catalog of RF pulses occurring during an event, but does not show the conductive channels connecting them. In order to reconstruct conductive channels, I use the principle that leaders may branch as they propagate, but do not merge. Consequently, each vertex in a leader can connect to any number of later vertices (representing branching), but at most one earlier vertex.

For each RF pulse, I find its nearest earlier neighbor and connect them. Additionally, because conductive channels may be reactivated by subsequent stepped or dart leaders, RF sources that occur along a pre-existing conductive channel are merged into that channel. In this way, conductive channels may be traced backward from their terminal vertices to their beginnings.

One consequence of this scheme is that conductive channels may overlap in the early sections of the leader. This is desirable because current flow through either will correctly imply thunder production from their overlapped section. In the case of multiple overlapping channels carrying current, the acoustic source amplitude of their overlapped sections will be the linear sum of the source amplitudes of the individual channels. This follows from the acoustic source amplitude being proportional to the current, which must be conserved throughout the channel structure.

The number of conductive channels to consider can be reduced (Figure 2.2) by eliminating “dead end” channels whose independent segments (i.e., segments that do not overlap with longer channels) are short. These dead ends are leaders that branched from another channel but failed to propagate far, and therefore are unlikely to carry current. Removing dead ends is advantageous for two reasons: it reduces the number of parameters in the model, and reduces the computational expense of modeling thunder signals. This process may decrease the number of channels from hundreds to less than ten, depending on the independent segment length threshold used for dead end identification. The threshold needed to eliminate dead ends but not the main channels depends on the scale of the strike; for each strike studied here, I picked an optimal threshold that reduced strike complexity while preserving core channels. Additionally, for CG events the entire

set of channels formed by downward-propagating leaders before the first return stroke must be considered because of the possibility of charge deposition along the entire structure during the first return stroke. Therefore, I include that structure (including dead ends) as a potential acoustic source in addition to the main channels identified by dead end elimination.

2.2 Acoustic Forward Modeling

Each conductive channel may be regarded as a string of finely spaced (in this work, every 1 m) acoustic point sources; this approximation is valid as long as the spacing is short compared to the wavelengths studied (from about 25 m to 60 m for the 6-12 Hz band studied here). For each point source, I use standard ray tracing equations (*Garces et al., 1998; Anderson, 2013*) to calculate travel time and arrival amplitude of signals from each point source. Time of thunder generation is determined by electromagnetic observations; in this work, I used electrical interference produced by lightning current flow and recorded by our unshielded sensor cables, but RF pulse timing could be used as well. Typically, multiple strokes are detected during a flash. However, the errors associated with propagation through complicated atmospheres make the relatively small intervals between strokes unresolvable. Therefore, only a single source time (the mean time of all strokes) is used in these calculations. I construct an “arrival function” by superposing impulses whose timing and amplitude correspond to those of arrivals associated with each point source.

To convert this arrival function into a true pressure signal, I would need to convolve it with a source time function, which is unconstrained. However, the channel heating and expansion that produces thunder occurs rapidly, and I

ultimately band pass filter these models and recordings to low frequencies, so the source time function can be treated as being approximately impulsive. Band-limiting also makes it unnecessary to account for attenuation, which has little effect on these low frequencies at these distances.

Phase coherence between recorded thunder and modeled signals is most likely weak for these frequencies, assuming inexact source time functions and atmospheres. Because of this, I calculate the power envelope of recorded and modeled signals before comparing them; this makes signal comparison less sensitive to small timing errors in modeled signals. This forward modeling procedure is repeated for each microphone in the network and each conductive channel, giving us a set of signals each microphone would record for each conductive channel.

2.3 Inversion for Channel Source Amplitudes

Thunder can be treated as a weighted superposition of different channels' acoustic signatures. To determine the weight of each channel, I concatenate signals for different microphones (so that all data to be fit are contained in a single vector) and perform a non-linear inversion using the Metropolis-Hastings Markov Chain Monte Carlo (MCMC) method (*Hastings, 1970; Aster et al., 2012*) to minimize the misfit between modeled and observed power envelopes. This method has important advantages over other nonlinear inverse methods, including its ability to return a posterior distribution of model parameters and its robustness against returning locally (not globally) optimal models. Using the notation \mathbf{G} for a matrix whose columns are forward-modeled thunder signals, \mathbf{m} for a vector of acoustic source amplitudes, \mathbf{r} for a recorded thunder time series, and E for the power envelope function, I invert for \mathbf{m} to minimize the misfit

$$\|E(\mathbf{G}\mathbf{m}) - E(\mathbf{r})\|_2 \tag{2.1}$$

This MCMC implementation consists of 50000 iterations in which a random model parameter is perturbed by multiplication by a positive random number drawn from a log-normal distribution centered at 1. Because negative parameter values indicate unrealistic rarefactions instead of compressions radiating from lightning channels, I require that all model parameters be non-negative. This method of parameter perturbation accomplishes that. In each iteration, misfit between modeled and recorded data is calculated. The proposed model parameter is always accepted if it decreases the misfit. Additionally, the proposed model parameter could be accepted if it increases the misfit, with probability of acceptance decreasing with higher differences in misfit. In practice, my acceptance ratio varied between 0.1 and 0.7. I have no prior information about the acoustic energy release of the lightning channels, and therefore use an uninformative prior. After running 50000 iterations, I consider the first 25000 to be a “burn-in” period in which the influence of the initial model has not been completely lost, and discard them. Then, to reduce correlation between successive iterations, only every tenth iteration is sampled. The models in these remaining iterations reflect the posterior distribution of the model.

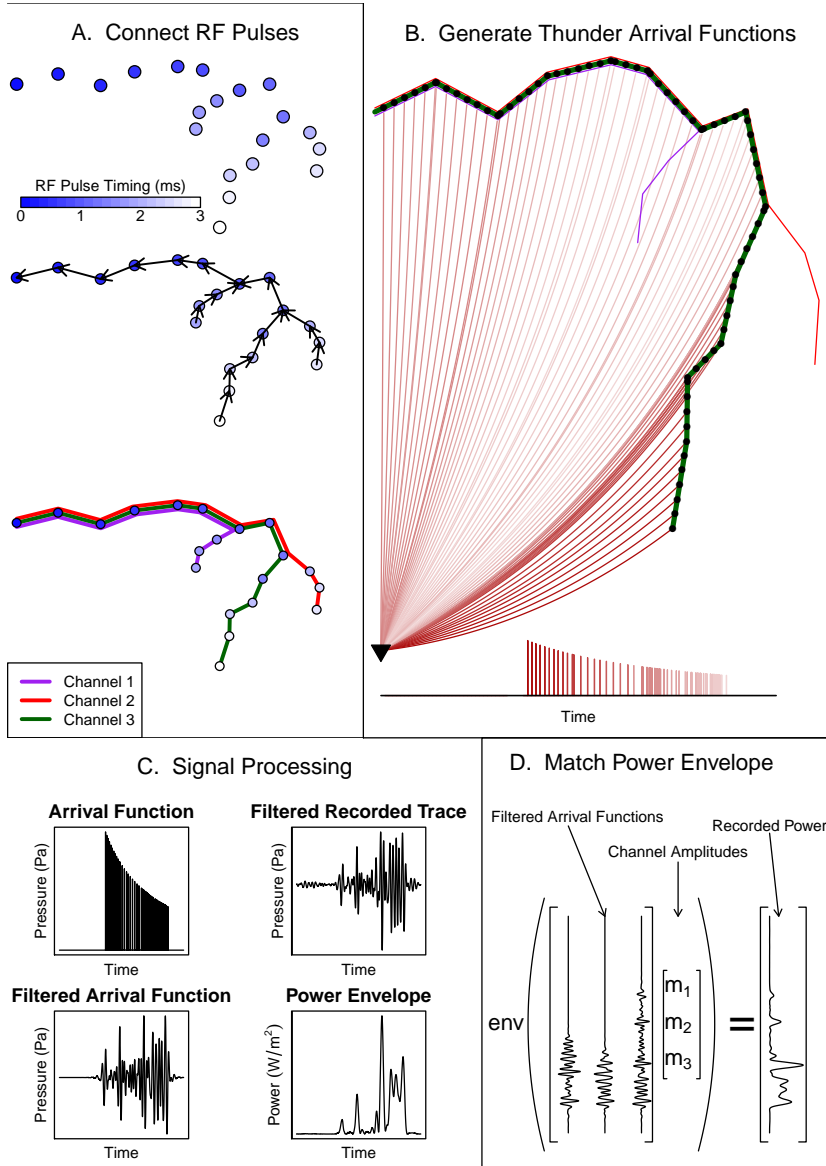


Figure 2.1: Schematic outline of the inversion method, using synthetic data. A: each RF pulse is connected to its nearest neighbor that occurs earlier in time. These connections can be traced backwards to reconstruct conductive channels. B: each channel (here, channel 3) is discretized as a set of finely spaced interpolated acoustic sources. Travel times and amplitudes are calculated for waves propagating from each source to the receiver. These arrivals are represented as time-shifted, amplitude-scaled delta functions, and are superposed to form an arrival function. C: arrival functions are filtered, and the power envelope is calculated for the filtered recorded data. D: a nonlinear inversion is performed to match the power envelope of a weighted superposition of filtered arrival functions to the power envelope of the recorded data.

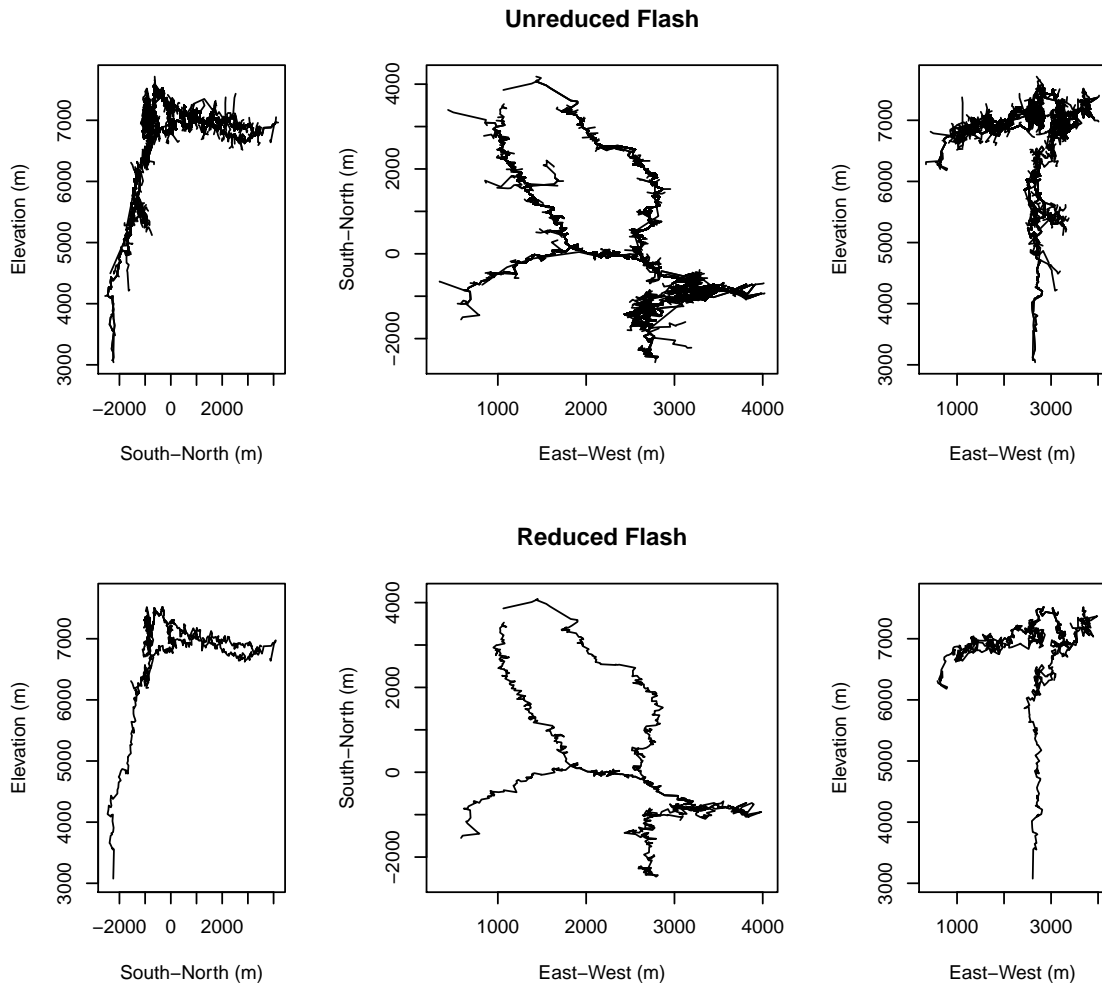


Figure 2.2: The number of channels in a flash can be reduced by discarding those with short independent length. This reduces the computational expense of forward-modeling thunder signals, as well as reducing the number of free parameters in the inverse problem. In this flash, the number of channels to consider was reduced from 431 to 7.

CHAPTER 3

EXPERIMENT

3.1 Deployment and Data

I analyze data from a 2009 instrument deployment in the Magdalena Mountains in central New Mexico. Twelve broadband (< 0.1 Hz to a Nyquist frequency of 500 Hz) Infra-NMT microphones with flat frequency responses (*Marcillo et al.*, 2012) were deployed in three arrays (MGTM, MKVH, and MLAN) consisting of four microphones each. Microphone arrays were in a triangular configuration with three peripheral and one central microphone connected by cable to a RefTek RT-130 data logger recording 1000 samples per second at 24 bits. Because of the close spacing of the microphones within the arrays, acoustic data from the central microphones only are considered here (although, for determining strike timing, electrical interference recorded on all acoustic channels is considered). Recordings were converted to overpressure units before analysis. Additionally, I used electromagnetic data from nine LMA sensors, with three forming a local component to the array (within 2 km of the acoustic network center), and another six forming a regional component (within 30 km of the acoustic network center). The LMA and microphone arrays both received precise timing information from GPS antennas.

I present results from several flashes during a storm that occurred on July 24, 2009. I examine in particular detail a CG flash that occurred at 19:42:13 UTC.

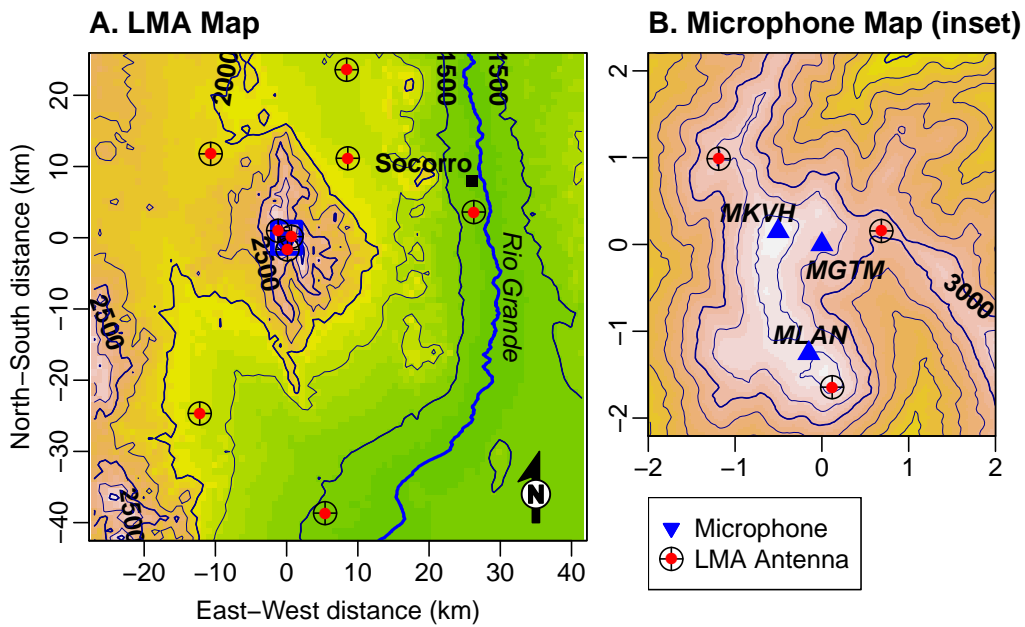


Figure 3.1: Map of sensor deployment used in this experiment in central New Mexico, USA. The LMA (A) consisted of a “regional” component consisting of six antennas spaced around the Magdalena Mountains at distances of more than 10 km and a “local” component including three antennas deployed close together high in the mountains. The acoustic network (B) included three broadband microphones deployed in the same area as the local part of the LMA (within the blue square). The MGTM station is used as the origin of the map.

This strike included 2555 RF sources that were connected to form 431 conductive channels. The vast majority of these channels are most likely inactive dead ends because of their short independent lengths. In order to simplify the strike and remove these channels from consideration, all channels whose independent length fell below a threshold of 4500 m were ignored; this reduced the number of potential current-carrying channels to seven. These seven include one that extends all the way to ground, one that extends downward but fails to reach ground, two that propagate from above to meet the top of the ground strike, and three that extend horizontally away from the ground strike at high elevation (Figure 3.2).

Low-frequency radio interference from five significant current pulses (as well as many more smaller current pulses) was detected during this flash (Figure 3.3). However, the time intervals separating these pulses (0.05-0.2 s) are short compared to the duration of thunder signals and to the likely timing errors associated with propagation through complex atmospheres. Therefore, I find the average time of all strokes and use it as the sole source time in these calculations.

For each flash, I performed a grid search over many windless atmospheres with constant vertical sound speed gradients to find an optimal fit. Sound speed gradient varied from -0.006 to -0.0036 s^{-1} and ground-level (3000 m above sea level) sound speed varied from 336 to 354 ms^{-1} . These correspond to temperature gradients of roughly $6\text{-}10 \text{ }^\circ\text{C} \cdot \text{km}^{-1}$ and ground-level temperatures of roughly $9\text{-}41 \text{ }^\circ\text{C}$. Each atmosphere was tested using the inversion method described in the previous chapter. After identifying the atmosphere with the best fit, I repeated the inversion on that atmosphere using 200000 iterations instead of 50000 and a burn-in period of 100000 instead of 25000. This was done in order to better characterize the posterior distribution of the model.

Additionally, I tested five frequency bands for the flash that occurred at 19:42:13. The low corner of these bands ranged from 3 to 12 Hz, and the high corner was set to twice the low corner. I found that a band from 6-12 Hz resulted in the lowest misfit for this flash. Additionally, synthetic data presented in the next chapter show that this band is the least susceptible to wind-related errors. Therefore, I picked this frequency band for analyzing other flashes.

3.2 Results

3.2.1 19:42:13 Flash

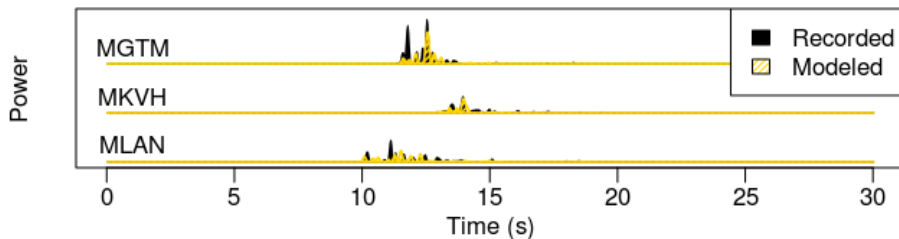
Detected thunder in this flash came from three mainly vertical channels extending toward ground (Figure 3.2). One of these is the original channel that extends from the initial breakdown to the ground; this produced the most thunder. Additionally, two subsequent channels formed from later breakdowns and connected to the top of the main ground strike; these produced much less thunder.

Interestingly, no thunder was detected from the long upper channels that propagated mainly horizontally. Considering the time of channel formation with respect to current pulse times (detected by low-frequency RF interference) can explain this finding (Figure 3.3). Glitches caused by RF interference synchronous with dart leaders are seen throughout the flash. More than half of these occur before the upper channels begin to form, and nearly all occur before the upper channels are fully formed. This indicates that these channels might not be major thunder sources because during most of the thunder-producing return strokes, the channels did not yet exist. On the other hand, the three channels that were found to produce thunder formed early in the strike.

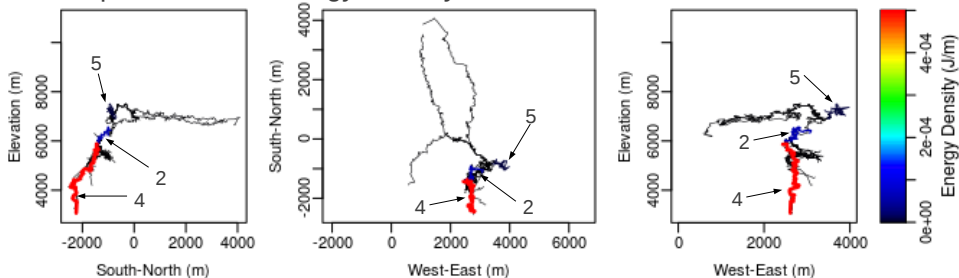
19:42:13 Flash

A. Model Fit to Data

RMS Misfit 0.723



B. Map of Channel Energy Density



C. Energy Density Posterior Distributions

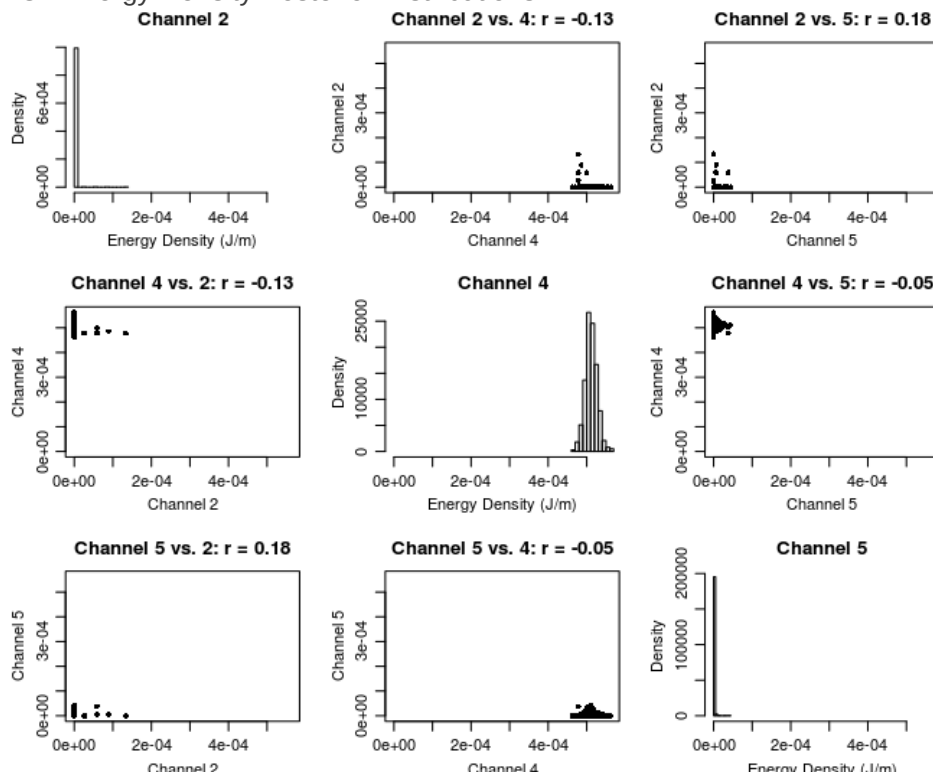


Figure 3.2: A: Overlay of modeled and recorded thunder power envelopes for the CG flash at 19:42:13. B: Map of inverted channel energy densities. C: Posterior distributions of channel energy densities of thunder-producing channels. Channel 4, which is the direct channel to ground, produces the most thunder. Channels 2 and 5, which connect channel 4 to higher parts of the strike, produce little thunder.

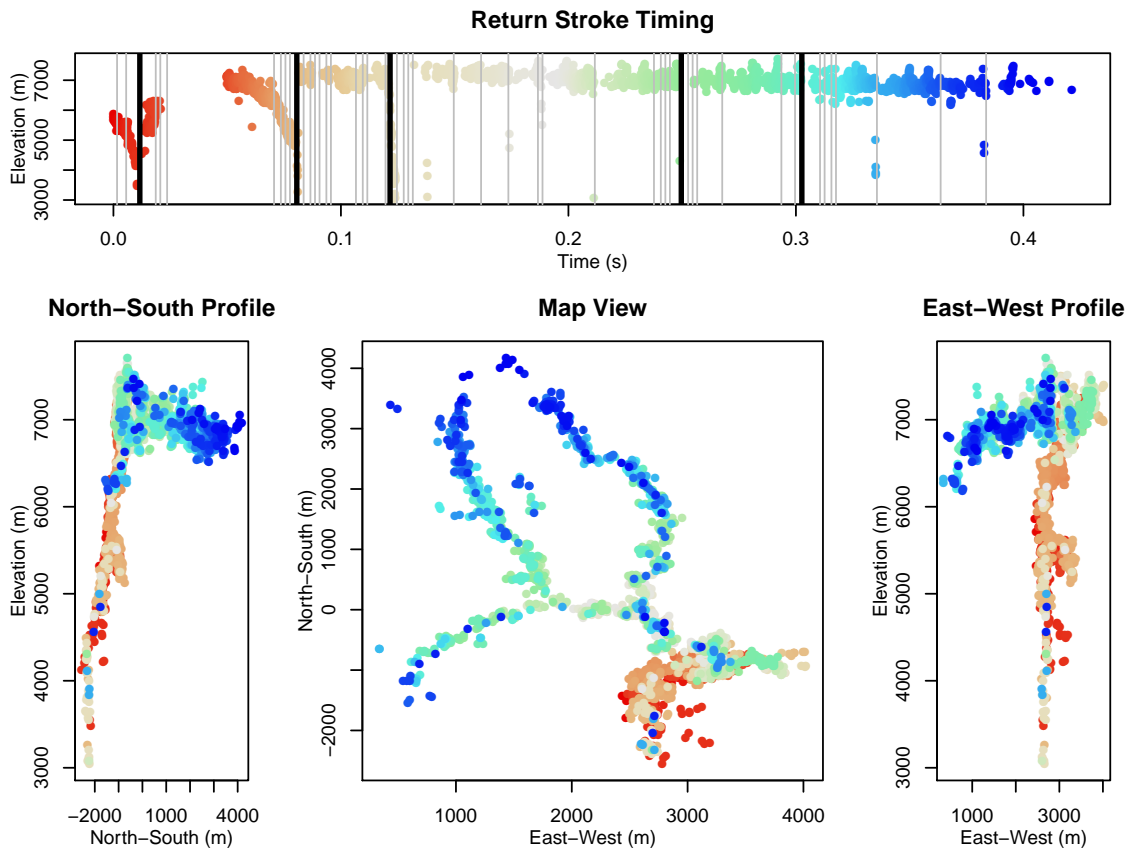


Figure 3.3: The evolution of the CG flash at 19:42:13 with time. Color of plotted points corresponds to VHF pulse times. Black vertical lines indicate times of major low-frequency radio pulses from return strokes; gray lines indicate smaller radio pulses. Most of the upper channels formed after the return strokes, making them unlikely to produce significant thunder.

3.2.2 19:06:36 Flash

This IC flash includes two downward-propagating channels, one channel that extends horizontally away from the initial breakdown, and one that extends upward (Figure 3.4). All of these except one of the lower channels were found to produce thunder, and the mid-level, horizontal channel was the most energetic. Recovered energy densities of the lower and upper channels have a moderate negative correlation of -0.3, meaning that fit to recorded thunder may be roughly preserved by increasing energy density of one and decreasing it for the other. As a result, it is difficult to determine exactly how acoustic energy is partitioned between those two channels.

3.2.3 19:14:41 Flash

This CG flash consists of a channel going to ground along with a few horizontally propagating upper channels (Figure 3.5). Thunder from this flash is fit relatively well by models (fractional rms misfit of 0.73). The ground strike is the most energetic channel, but two upper channels also produce substantial thunder. However, the recovered energy densities of the two upper channels are correlated ($r = -0.39$), meaning that energy density can be allocated to either and have a relatively small effect on model misfit.

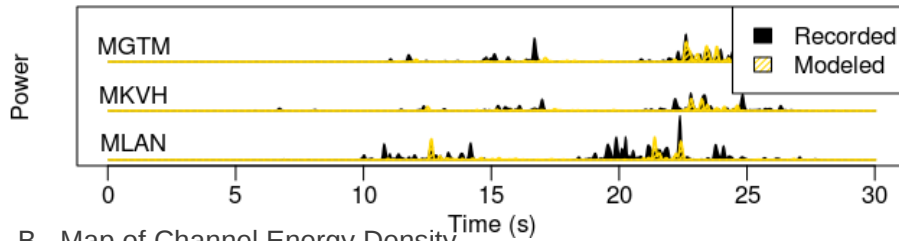
3.2.4 19:32:51 Flash

This IC flash consists of one main low-level channel, two upper-level channels, and a single connection between the layers (Figure 3.6). One of the upper channels is calculated to produce the most thunder. A second upper channel and

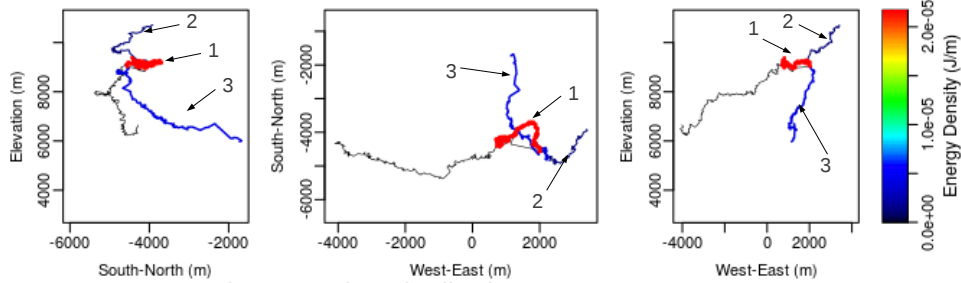
19:06:36 Flash

A. Model Fit to Data

RMS Misfit 0.841



B. Map of Channel Energy Density



C. Energy Density Posterior Distributions

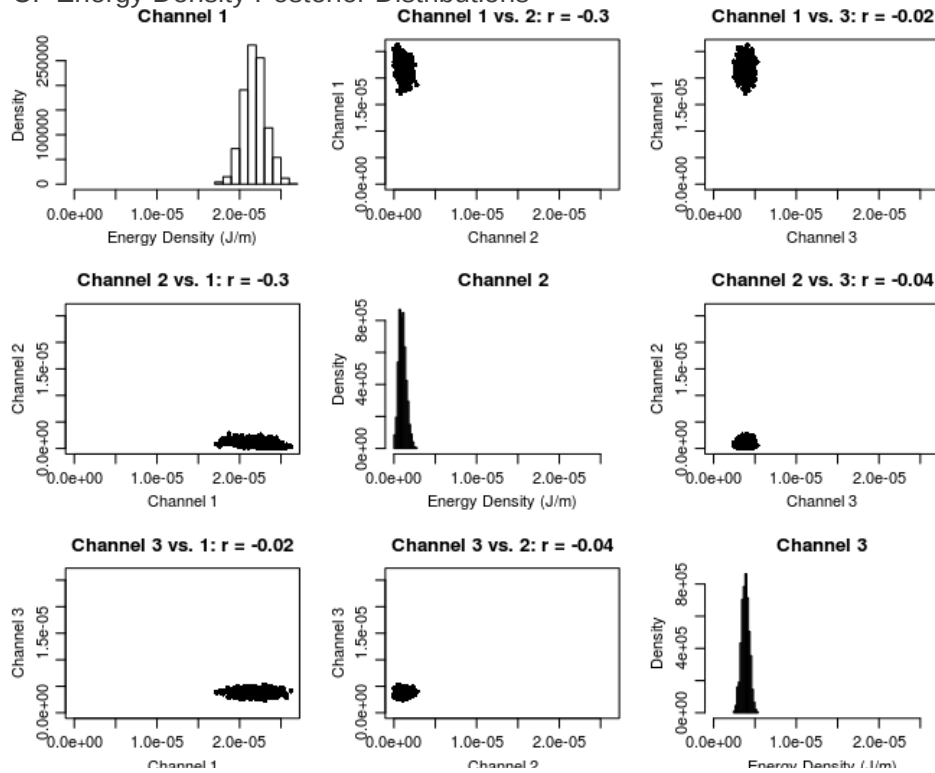
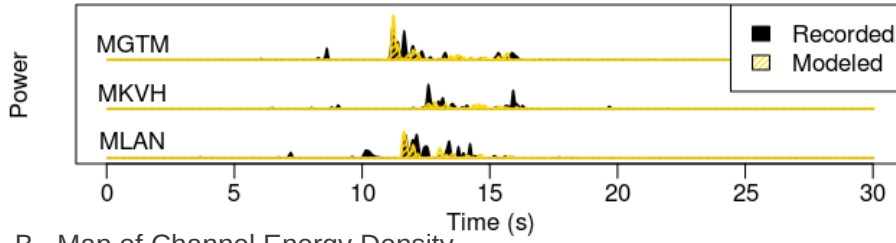


Figure 3.4: A: Overlay of modeled and recorded thunder power envelopes for the IC flash at 19:06:36. B: Map of inverted channel energy densities for the flash. C: Posterior distributions of channel energy densities of thunder-producing channels. Channels 1 and 2 are somewhat correlated; this is a potential source of ambiguity in the results.

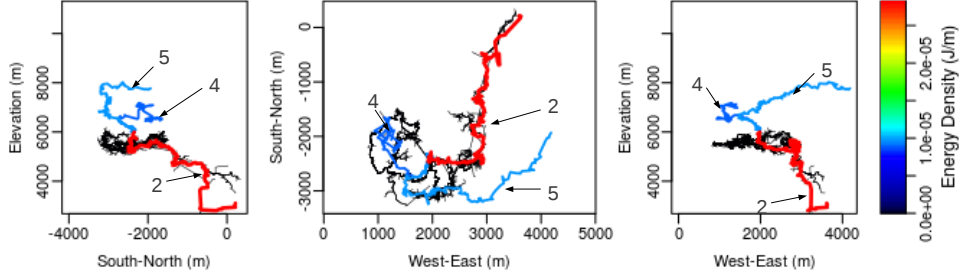
19:14:41 Flash

A. Model Fit to Data

RMS Misfit 0.73



B. Map of Channel Energy Density



C. Energy Density Posterior Distributions

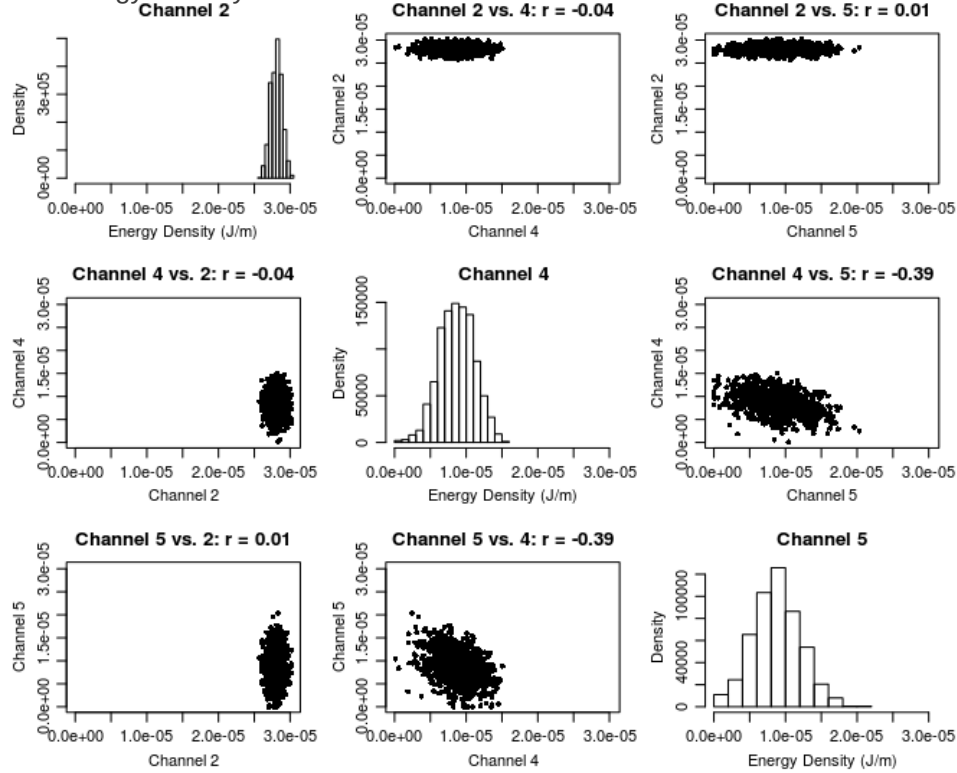


Figure 3.5: A: Overlay of modeled and recorded thunder power envelopes for the 19:14:41 CG flash. B: Map of inverted channel energy densities. The ground strike has the highest energy density; however, thunder is also detected from two upper channels. C: Posterior distributions of channel energy densities. Energy densities of two upper channels are correlated, making distinguishing thunder from them difficult.

the low channel also produce measurable thunder. Fit of models to observations is relatively poor (rms misfit of 0.9), meaning that much of the thunder cannot be explained by this method.

3.2.5 19:50:08 Flash

This IC flash includes two high-elevation channels and two lower channels (Figure 3.7). Of these, only one channel (an upper channel) is found to produce any thunder. However, the misfit is high (0.936), meaning that some thunder-producing channels are not being identified because of unmodeled effects on waves they produce.

3.2.6 19:54:19 Flash

This IC flash also consists of two upper channels and two lower channels (Figure 3.8). Thunder is detected prominently from one of the upper channels and ambiguously from a lower channel. The fit between modeled and recorded thunder is moderate (0.806).

19:32:51 Flash

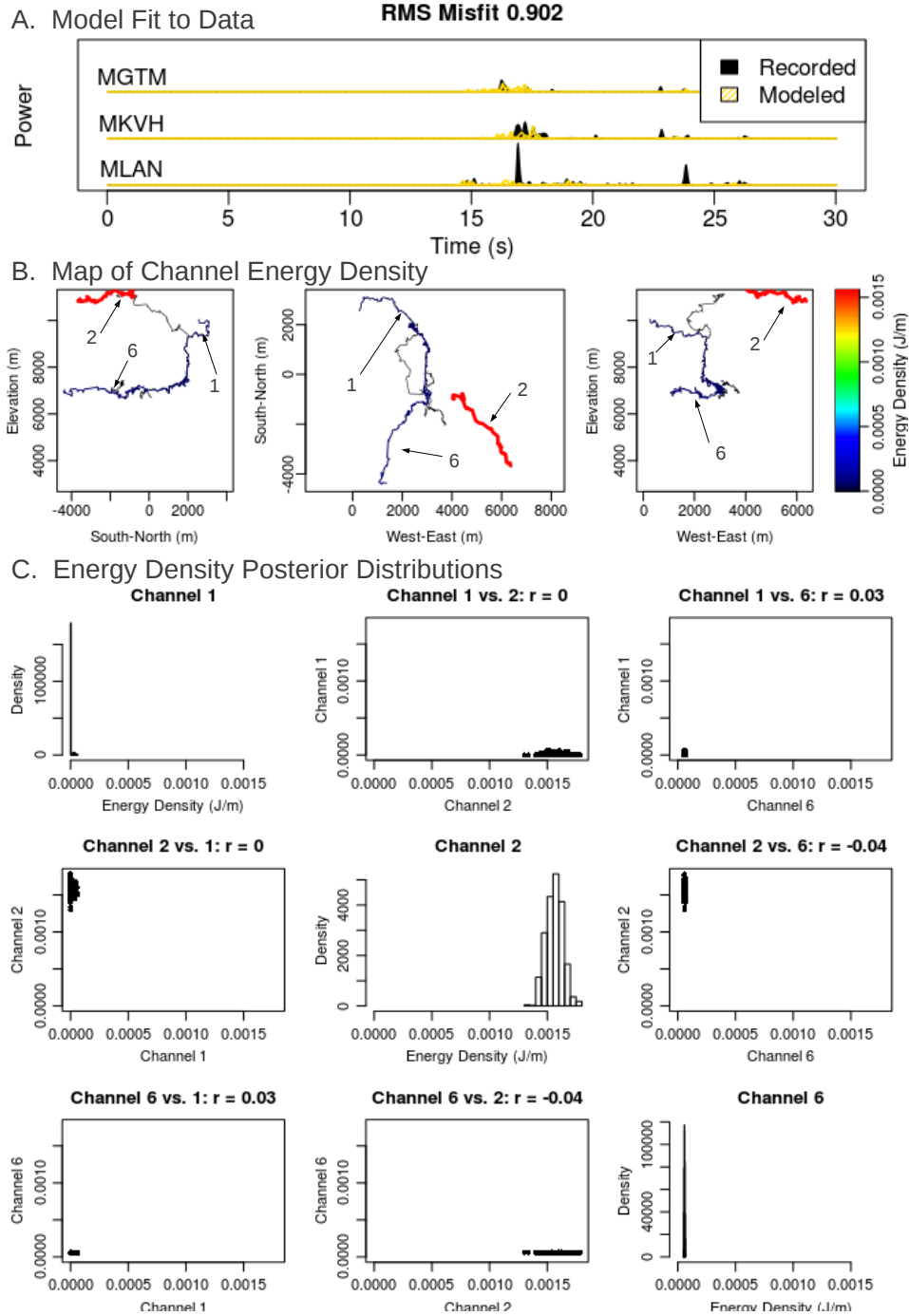
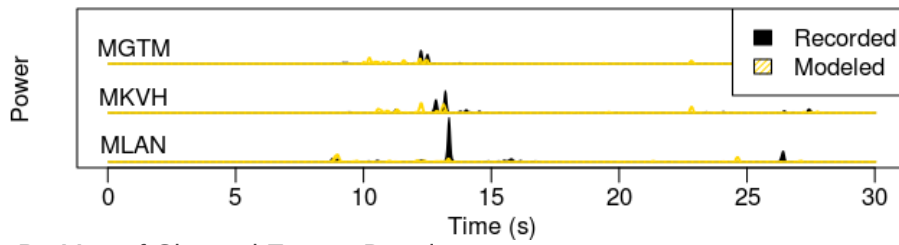


Figure 3.6: A: Overlay of modeled and recorded thunder power envelopes for the 19:32:51 IC flash. B: Map of inverted channel energy densities. Most energy is released by a high-elevation channel, but small amounts are also produced by other channels. C: Posterior distributions of channel energy densities of thunder-producing channels.

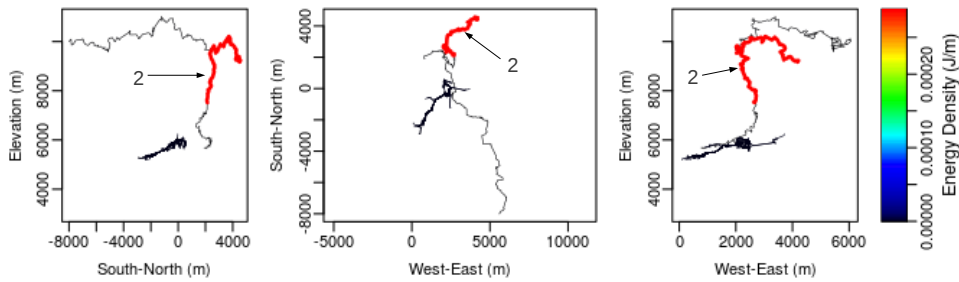
19:50:08 Flash

RMS Misfit 0.936

A. Model Fit to Data



B. Map of Channel Energy Density



C. Energy Density Posterior Distributions

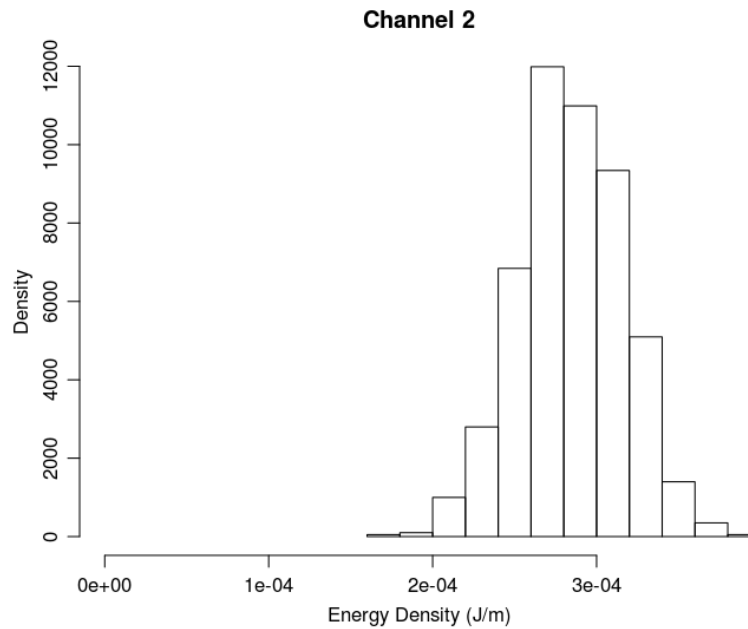
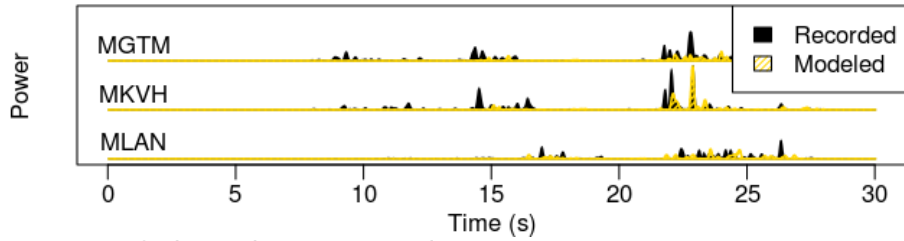


Figure 3.7: A: Overlay of modeled and recorded thunder power envelopes for the 19:50:08 IC flash. B: Map of inverted channel energy densities. C: Posterior distributions of channel energy densities of thunder-producing channels. Only one channel is found to produce any thunder.

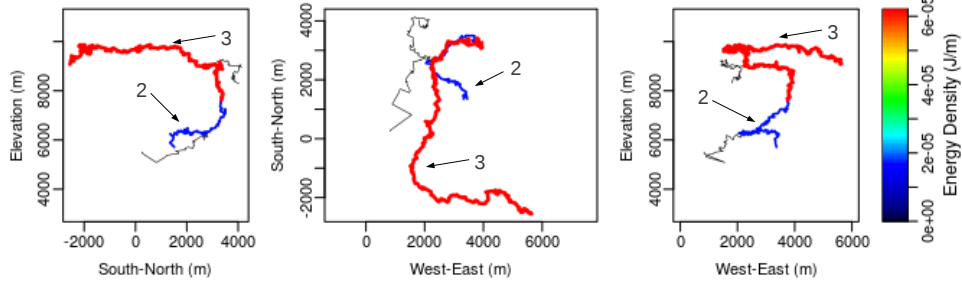
19:54:19 Flash

RMS Misfit 0.806

A. Model Fit to Data



B. Map of Channel Energy Density



C. Energy Density Posterior Distributions

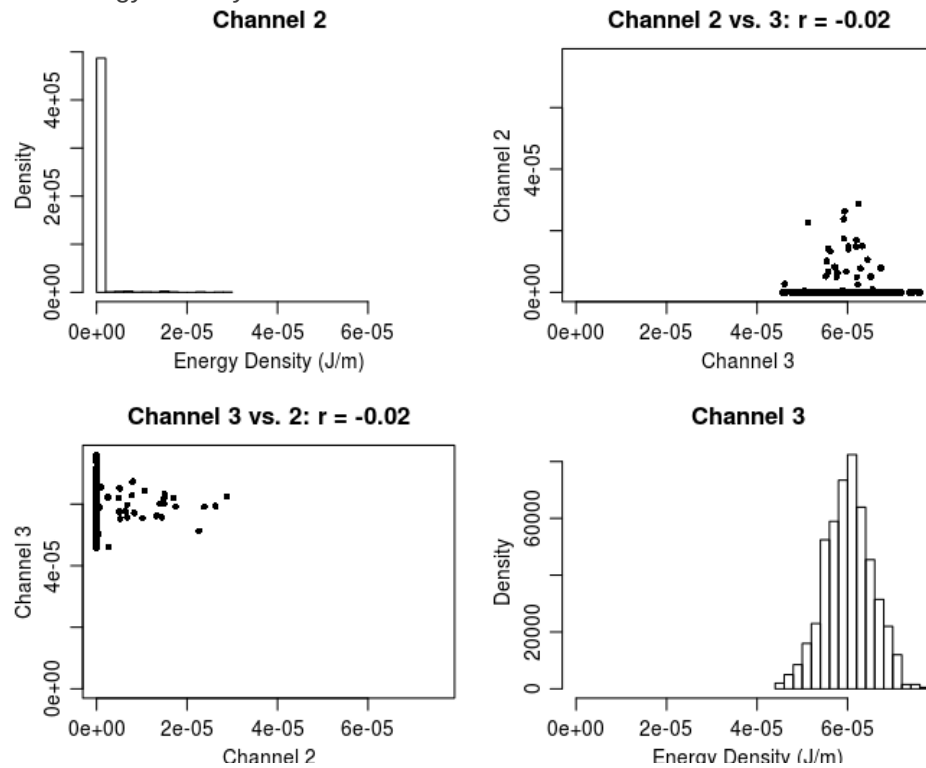


Figure 3.8: A: Overlay of modeled and recorded thunder power envelopes for the 19:54:19 IC flash. B: Map of inverted channel energy densities. C: Posterior distributions of channel energy densities of thunder-producing channels. An upper channel (3) produces most thunder; contributions from the lower channel (2) are smaller and poorly resolved.

CHAPTER 4

SENSITIVITY OF METHOD TO SOURCES OF ERROR

Monte Carlo simulations were performed in order to assess the importance of potential sources of error affecting this method. The main sources of error are location uncertainty of RF sources located by the LMA (addressed in Section 4.1) and the unknown structure of the atmosphere (Section 4.2). In each simulation, synthetic thunder was modeled for a realistic lightning strike (using the geometry of the 19:42:13 flash) and atmosphere. I then attempted to invert this signal for channel amplitude after adjusting the strike or atmosphere for each source of error. Several error intensities and band-pass filter frequency bands were tested; inversions were repeated several times for each error intensity and frequency combination.

4.1 Sensitivity to RF pulse location noise

RF pulse locations provided by the LMA inevitably contain some noise. *Thomas et al.* (2004) found that typical horizontal and vertical location errors had standard deviations of 10 m and 30 m, respectively. These errors will affect travel times of modeled acoustic waves and alter thunder signals accordingly. Here, I quantify the effect of RF pulse location noise on thunder signal recovery.

Twenty independent iterations were run for each filter and location noise level. In each iteration, thunder was forward modeled for the original RF pulse

locations using the main downward-reaching channel as the sole source. Then, RF pulses were offset by random errors distributed according to the standard deviations being tested. Finally, the modeled thunder and offset RF pulse locations were inverted. Two quantities were recorded: the rms misfit between the initial thunder and the inverted thunder, and the rms error between the true and inverted channel source amplitudes. I tested eight location standard deviations and six bandpass filters. Horizontal standard deviations ranged from 1 m to 215 m, with vertical standard deviation set to three times the horizontal standard deviation. Frequency band high corners ranged from 1.4 Hz to 8 Hz, with each low corner set to one-half the high corner.

Figure 4.1 shows the dependence of misfit on frequency band and location standard deviation. The fractional misfit,

$$M_{true} = \frac{\|E(\mathbf{G}\mathbf{m}_{true}) - E(\mathbf{r})\|_2}{\|E(\mathbf{r})\|_2} \quad (4.1)$$

was calculated for each simulation, and mean fractional misfits were calculated for each frequency-standard deviation pair and contoured.

Additionally, I examine the effect of RF pulse location noise on accuracy of inverted channel amplitudes. RMS distance between true and inverted channel amplitudes (when active channels have an amplitude of 1) is strongly dependent on RF pulse location noise, and, to a lesser extent, corner frequency. These errors are generally between 0.125 and 0.25 for near-infrasound corner frequencies and realistic RF pulse location noise values.

4.2 Sensitivity to atmospheric simplification

Thunderstorm atmospheric structure is complex, dynamic, and typically unknown. It is obviously impossible to test every possible sound speed structure.

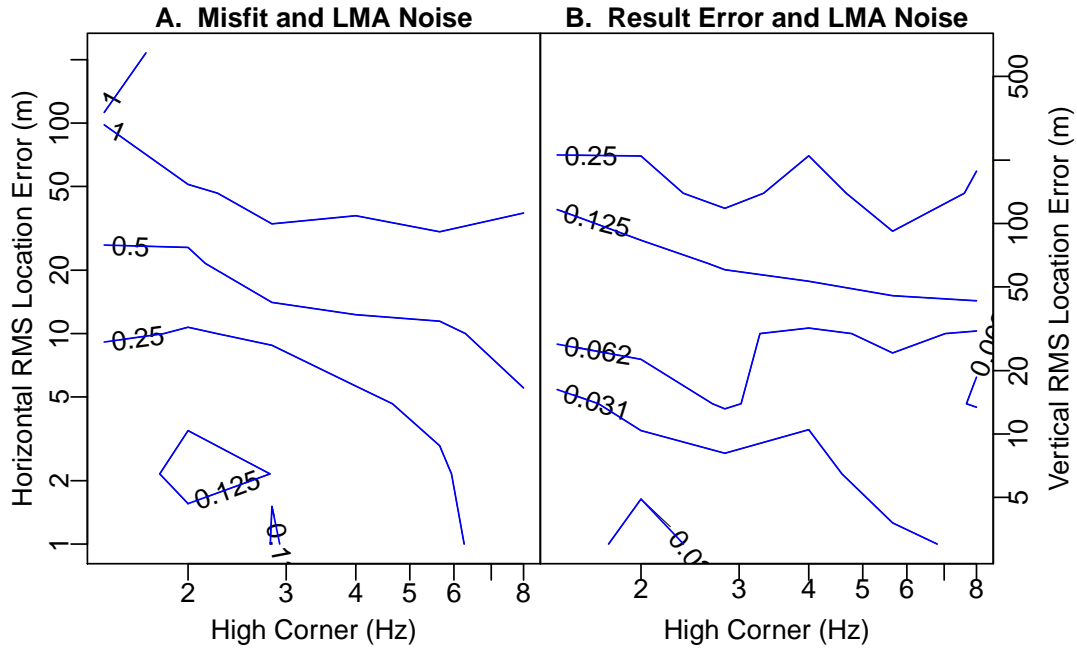


Figure 4.1: Contours showing the effect of LMA RF pulse location noise on inversions of synthetic data. Monte Carlo simulations revealed effects on (A) fractional misfit between pre-noise and post-noise synthetic thunder and (B) errors between true and inverted amplitude (expressed as root-mean-square residual between true and inverted amplitudes). Fractional thunder misfits increase with both the RMS location error and the corner frequency. However, errors in inverted channel amplitudes depend more strongly on RMS location error than on corner frequency.

As a result, the difference between the tested atmosphere and true atmosphere constitutes an important source of noise.

I use a similar procedure to the two previous tests. The atmosphere from which thunder is generated is allowed to vary, with a realistic and constant temperature structure (surface sound speed of 343 ms^{-1} and vertical sound speed gradient of -0.005 s^{-1}) and six different windiness levels. For each windiness level, 12 simulations were run. In each simulation, surface wind in a random direction was set to a random speed with random shears chosen from an interval that depended on the windiness level being tested. The maximum allowable surface wind and shear were 7 ms^{-1} and 0.0175 s^{-1} . Six frequency bands were then tested to determine how filtering affected results.

Thunder misfit increases rapidly with windiness and corner frequency (Figure 4.2). However, for low levels of wind (surface wind less than 3 ms^{-1} , wind shear less than 0.0075 s^{-1}), accuracy of inverted channel amplitudes was moderate (0.25-0.45 fractional rms), and could be higher for stronger winds. The frequency band with a high corner of 12 Hz seemed the least susceptible to wind-related errors over low windiness levels.

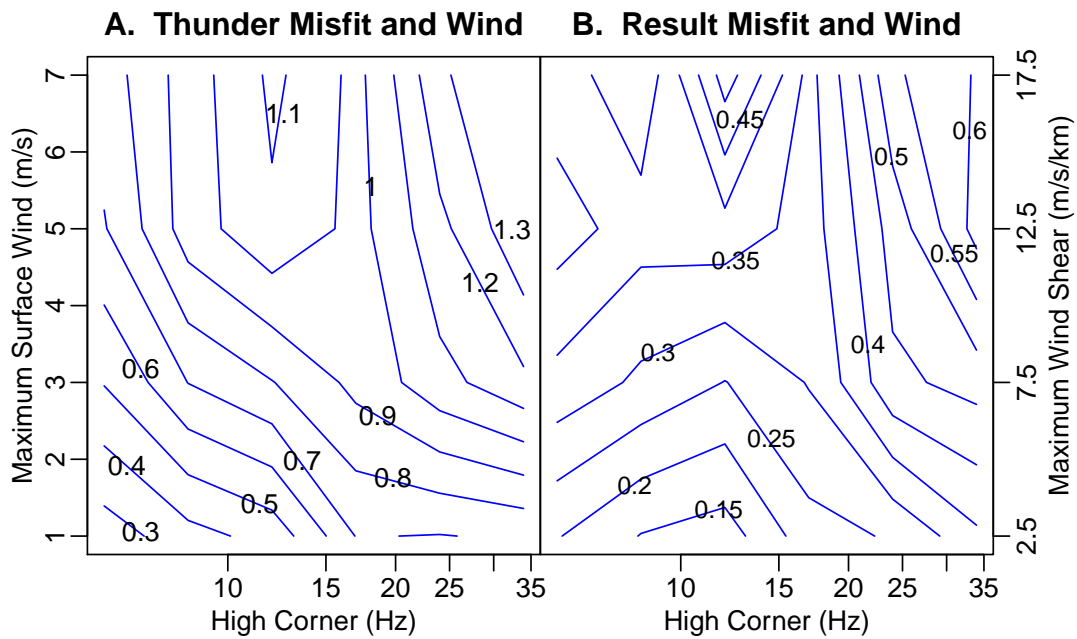


Figure 4.2: Effect of atmospheric wind intensity on (A) fractional misfit between true synthetic and inverted synthetic thunder and (B) accuracy of inverted channel amplitudes. Thunder misfit increases with corner frequency and maximum surface wind. However, true channel amplitudes can still be recovered reasonably accurately for low frequency bands.

CHAPTER 5

DISCUSSION

Misfit between modeled and observed thunder varied among flashes (Table 5.1). I calculated fractional RMS misfits as low as 0.723 and as high as 0.936. So, for some flashes, thunder could be reproduced fairly well, while for other flashes, little of the thunder could be modeled. Notably, CG flash thunder was reproduced much more reliably than IC thunder: misfits for both CG flashes were lower than misfits of any IC flashes. This could be related to the acoustic sources in IC flashes being higher (and therefore, more susceptible to atmospheric propagation effects) than those in CG flashes.

The geometry of inverted acoustic sources in CG flashes is reasonable. In each CG flash studied, the channel from the initial breakdown toward ground was the most energetic acoustic source, while some higher channels produced thunder as well. Because the channel to ground is necessarily involved in all return strokes, whereas upper channels may be involved in some or even none, I expect that the ground channel would be the loudest channel. In the flash at 19:42:13, the ground channel's energy density is much greater than the sum of the upper channels' energy densities. This indicates that most current flowed through the ground channel only, and that the return strokes carried by the upper channels were much less energetic. The CG flash at 19:14:41, on the other hand, has upper channels whose energy density sum is only slightly less than the energy density

	Time (UTC)	Type	Thunder-Producing Channels	RMS Misfit	Energy Density (Jm^{-1})	Total Energy (J)
1	19:06:36	IC	3	0.937	2.17×10^{-5}	0.218
2	19:14:41	CG	3	0.745	2.82×10^{-5}	0.537
3	19:32:51	IC	3	0.869	0.00156	12.3
4	19:42:13	CG	3	0.74	5.00×10^{-4}	3.3
5	19:50:08	IC	1	0.924	2.88×10^{-4}	3.06
6	19:54:19	IC	2	0.977	6.2×10^{-5}	1.72

Table 5.1: Summary of lightning flashes studied. Data are from a July 24, 2009 thunderstorm. RMS misfit, energy density, and total energy refer to values obtained by analyzing the 6-12 Hz frequency band.

of the ground channel. This indicates that the upper channels were active during the most energetic return strokes, and most current flowed through both an upper and lower channel.

Because IC flashes do not involve a large conductive charge reservoir, their current pulses are less predictable. Consequently, it is difficult to assess whether a thunder source geometry for an IC event is reasonable. In the flash at 19:50:08, only a single channel was found to produce any thunder at all. However, in the 19:06:36 flash, three of the four channels produced substantial thunder. Fractional misfits between recorded and modeled thunder are somewhat high in these flashes—no flash has a fractional misfit less than 0.72, and no IC flash has a fractional misfit less than 0.8. However, in the previous chapter, I determined that sources of error like VHF pulse location uncertainty and atmospheric winds could cause substantial thunder misfit while still allowing reasonably accurate estimates of source energy density. For example, assuming that wind is the main source of error, a ground level wind of 3 ms^{-1} and a shear of $7.5 \times 10^{-3} \text{ s}^{-1}$ could cause a fractional thunder misfit of 0.8, but a fractional source amplitude error of only 0.25 (Figure 4.2). High thunder misfits do not necessarily indicate

similarly inaccurate source energy estimates.

Other sources of error, such as echoes off topography and atmospheric heterogeneities more complicated than one-dimensional linear variations with elevation could potentially reduce the accuracy of this method. For example, a ground-level inversion could preferentially focus waves from low-elevation sources to receivers. Wave propagation models would not predict this and would therefore overestimate energy density of low channels while underestimating high channels. Similarly, a local vertical wind or turbulent region might distort thunder signals from nearby channels, causing those channels' source energies to be underestimated by the inversion. Topographic echoes might have the opposite effect: the coincident arrival of direct waves from one channel and a topographic echo from a different channel could not be predicted without a more complex propagation model; without one, all arriving energy would be attributed to the direct waves, and the energy of the channel producing them would be overestimated.

Finally, the energy densities recovered in this work (between $2 \times 10^{-5} Jm^{-1}$ and $1.5 \times 10^{-3} Jm^{-1}$) may seem extremely low for lightning strikes carrying current on the order of $3 \times 10^4 A$ (Table 5.1). However, several factors must be considered. First is that the channels are very long (thousands of meters) and energy is radiated along its entire length, so the total energy released is, in these units, 3-4 orders of magnitude higher than the energy density. Further, I am only looking at a narrow frequency band (6-12 Hz) that carries only a small fraction of the total thunder energy. Finally, thunder generation is highly inefficient: most input energy is dissipated in shock wave decay close to the channel. So these seemingly low thunder energy densities do not conflict with the enormous amount of energy involved in lightning.

CHAPTER 6

CONCLUSION

I have introduced a new method for locating thunder sources and current flow within a lightning flash by joint inversion of synchronous thunder recordings and RF pulse catalogs from the LMA. This method involves connecting RF pulses to reconstruct conductive channels created by leaders, modeling acoustic signals produced by each conductive channel, and inverting using a Monte Carlo Markov Chain to determine the source energy density of each conductive channel in order to minimize misfit between modeled and recorded thunder power envelopes. The returned posterior distribution of channel energy density can be used to distinguish thunder-producing channels from silent channels.

Sources of error in this method include LMA RF pulse location noise and complications in atmospheres. Typical levels of LMA RF pulse location noise have little effect on accuracy of recovered channel energy densities. The effect of high winds is more significant. Additionally, effects of turbulence and topography could cause errors that are difficult to quantify, while intrinsic attenuation could potentially cause errors for frequencies higher than those studied here.

I applied this method to lightning flashes that occurred on July 24, 2009 in the Magdalena Mountains, New Mexico, USA. Thunder from CG flashes was reproduced more reliably than thunder from IC flashes. The misfit observed in some flashes is similar to expected values for moderately windy atmospheres,

for which source energy estimate errors are expected to be close to 25%. In most strikes, multiple channels produced thunder, and in all strikes, at least one channel produced no thunder.

This method has obvious applications in lightning research. Combining radio frequency and acoustic recordings will make locating current flow in flashes possible, much as the development of the LMA enabled the mapping of leader propagation. Better constraints on atmospheric structure in the vicinity of flashes (by radiosondes, for example) will improve the accuracy of this method and reduce the computational expense of testing many atmospheres.

REFERENCES

- Anderson, J., *AtmRay: Acoustic Traveltime Calculations for 1-D Atmospheric Models*, 2013, R package version 1.31.
- Arechiga, R. O., J. B. Johnson, H. E. Edens, R. J. Thomas, and W. Rison, Acoustic localization of triggered lightning, *Journal of Geophysical Research*, 116, D09,103, 2011.
- Aster, R. C., B. Borchers, and C. H. Thurber, *Parameter Estimation and Inverse Problems*, Elsevier Academic Press, 2012.
- Balachandran, N. K., Infrasonic signals from thunder, *Journal of Geophysical Research*, 84, 1735–1745, 1979.
- Balachandran, N. K., Acoustic and electric signals from lightning, *Journal of Geophysical Research*, 88, 3879–3884, 1983.
- Berdeklis, P., and R. List, The ice crystal-graupel collision charging mechanism of thunderstorm electrification, *Journal of the Atmospheric Sciences*, 58, 2751–2770, 2001.
- Bohannon, J. L., A. A. Few, and A. J. Dessler, Detection of infrasonic pulses from thunderclouds, *Geophysical Research Letters*, 4, 49–52, 1977.
- Byers, H., and R. Braham, Thunderstorm structure and circulation, *Journal of Meteorology*, 5, 71 – 86, 1948.
- de Groot-Hedlin, C., Finite-difference time-domain synthesis of infrasound propagation through an absorbing atmosphere, *Journal of the Acoustical Society of America*, 124, 1430–1441, 2008.
- Few, A. A., Power spectrum of thunder, *Journal of Geophysical Research*, 74, 6926–2934, 1969.
- Few, A. A., Lightning channel reconstruction from thunder measurements, *Journal of Geophysical Research*, 75, 7517–7523, 1970.
- Few, A. A., Thunder signatures, *EOS, Transactions AGU*, 55, 508–514, 1974.
- Few, A. A., and T. L. Teer, The accuracy of acoustic reconstruction of lightning channels, *Journal of Geophysical Research*, 79, 5007–5011, 1974.
- Fleagle, R. G., The audibility of thunder, *Journal of the Acoustic Society of America*, 21, 411–412, 1949.

- Garces, M. A., R. A. Hansen, and K. G. Lindquist, Traveltimes for infrasonic waves propagating in a stratified atmosphere, *Geophysical Journal International*, 135, 255–263, 1998.
- Hastings, W. K., Monte carlo sampling methods using Markov chains and their applications, *Biometrika*, 57, 97–109, 1970.
- Holmes, C. R., M. Brook, P. Krehbiel, and M. R., On the power spectrum and mechanism of thunder, *Journal of Geophysical Research*, 76, 2106 – 2115, 1971.
- Johnson, J. B., R. O. Arechiga, R. J. Thomas, H. E. Edens, J. F. Anderson, and R. L. Johnson, Imaging thunder, *Geophysical Research Letters*, 38, L19,807, 2011.
- Johnson, R. J., Characteristics of thunder and relationships to lightning sources in the magdalena mountains, central new mexico, Master's thesis, New Mexico Institute of Mining and Technology, Socorro, New Mexico, USA, 2012.
- MacGorman, D. R., A. A. Few, and T. L. Teer, Layered lightning activity, *Journal of Geophysical Research*, 86, 9900–9910, 1981.
- Marcillo, O., J. B. Johnson, and D. Hart, Implementation, characterization, and evaluation of an inexpensive low-power low-noise infrasound sensor based on a micromachined differential pressure transducer and a mechanical filter, *Journal of Atmospheric and Oceanic Technology*, 29, 1275–1284, 2012.
- Otterman, J., Finite-amplitude propagation effect on shock-wave travel times from explosions at high altitudes, *Journal of the Acoustical Society of America*, 31, 470–474, 1959.
- Rakov, V. A., and M. A. Uman, *Lightning: Physics and Effects*, Cambridge University Press, 2003.
- Reynolds, S. E., M. Brook, and M. F. Gourley, Thunderstorm charge separation, *Journal of Meteorology*, 14, 426–436, 1957.
- Rison, W., R. J. Thomas, P. R. Krehbiel, T. Hamlin, and J. Harlin, A GPS-based three-dimensional lightning mapping system: initial observations in central New Mexico, *Geophysical Research Letters*, 26, 3573–3576, 1999.
- Sutherland, L. C., and H. E. Bass, Atmospheric absorption in the atmosphere up to 160 km, *Journal of the Acoustical Society of America*, 115, 1012–1032, 2004.
- Teer, T. L., and A. A. Few, Horizontal lightning, *Journal of Geophysical Research*, 79, 3436–3441, 1974.
- Thomas, R. J., P. R. Krehbiel, W. Rison, S. J. Hunyady, W. P. Winn, T. Hamlin, and J. Harlin, Accuracy of the lightning mapping array, *Journal of Geophysical Research*, 109, D14,207, 2004.
- Uman, M. A., *The Lightning Discharge*, Orlando: Academic Press, 1987.

Valine, W. C., and E. P. Krider, Statistics and characteristics of cloud-to-ground lightning with multiple ground contacts, *Journal of Geophysical Research Atmospheres*, 107, 4441, 2002.

Weisman, M. L., and J. B. Klemp, The dependence of numerically simulated convective storms on vertical wind shear and buoyancy, *Monthly Weather Review*, 110, 504 – 520, 1982.